Steady State Calculations of Stationary Gas Tungsten Arc Welding from A Unified Arc-Electrodes Model †

TANAKA Manabu*, TERASAKI Hidenori**, USHIO Masao**** and John J. LOWKE****

Abstract

In order to clarify the formative mechanism of weld penetration in an arc welding process, the development of a numerical model of the process is quite useful for understanding quantitative values of the balances of mass, energy and force in the welding phenomena, because there is still a lack of understanding due to the existence of complicated interactive phenomena between the arc plasma and the weld pool. The present paper is focused on a stationary gas tungsten arc (GTA) welding process for simplification, but the whole region of GTA welding, namely, tungsten cathode, arc plasma, work-piece and weld pool is treated in a unified numerical model so as to take into account the close interaction between the arc plasma and the weld pool. The two-dimensional distributions of temperature and velocity in the whole region of GTA welding process are predicted. The weld penetration geometry is also predicted.

KEY WORDS: (Numerical model) (Calculation) (GTA) (Welding) (Arc) (Electrode) (Weld pool)

1. Introduction

Heat transfer from the arc plasma to the weld pool plays an important role in determing the weld penetration in arc welding [1]. Details of the fluid flow in the weld pool would be important in determining weld geometry. Taking account of all these phenomena is necessary for the development of a numerical model of the gas tungsten arc (GTA) welding process because there is close interaction between the arc plasma and the weld pool. For example, there are four driving forces of fluid flow in the weld pool [2]. These are the drag force of the cathode jet on the liquid surface, the buoyancy force, the electromagnetic force due to the self-magnetic field of the welding current, and the surface tension of the weld pool, as shown in **Fig. 1** [2]. These driving forces are dependent not only on the physical properties of the weld metal but also the properties of the plasma state [1]. Therefore, a unified numerical model accounting for both plasma and weld metal processes is important for predicting the GTA welding properties.

Modeling the arc welding process has been tried by a number of researchers [2-15]. However, almost every numerical model has treated either only the arc plasma [3-8] or only the weld pool [2,9-13]. Recently, modeling the combined arc plasma and the weld pool phenomena has been tried for stationary welding [14-15], but the calculated results of the arc plasma and the weld pool were made separately, without interaction between the plasma and the weld pool.

In the present paper, we use a unified numerical model of stationary GTA welding. The basic model and procedure is that of Sansonnens et al [16], but extended to include melting of the anode, with inclusion of convective effects in the weld pool. We give predictions of the two-dimensional distributions of temperature and velocity in the whole region of GTA welding process and also the predicted profile of weld penetration. We did not take into consideration metal vapor phenomenon from the weld pool or depression of the weld pool surface.

2. A Unified Arc-Electrode Model

The tungsten cathode, arc plasma and anode are described relative to a cylindrical coordinate, assuming rotational symmetry around the arc axis. The calculation domain is shown in **Fig. 2**. The domain of computation is divided into 95 nodes axially and 70 nodes radially, using a non-uniform grid. The flow is assumed to be laminar, the electron and heavy particle temperature are assumed to be equal and the effects of the non-collisional space-charged zone in front of both electrodes are neglected. Furthermore, the anode surface is assumed to be flat and unperturbed by the arc pressure. The diameter of the tungsten cathode is 3.2 mm with a 60 degrees conical tip. The shielding gas of GTA welding process is assumed to be pure argon.

† Received on July 31, 2002
* Assistant Professor
** Ph. D. Student
*** Professor
**** Honor Research Scientist, CSIRO, Australia

Transactions of JWRI is published by Joining and Welding Research Institute of Osaka University, Ibaraki, Osaka 567-0047, Japan

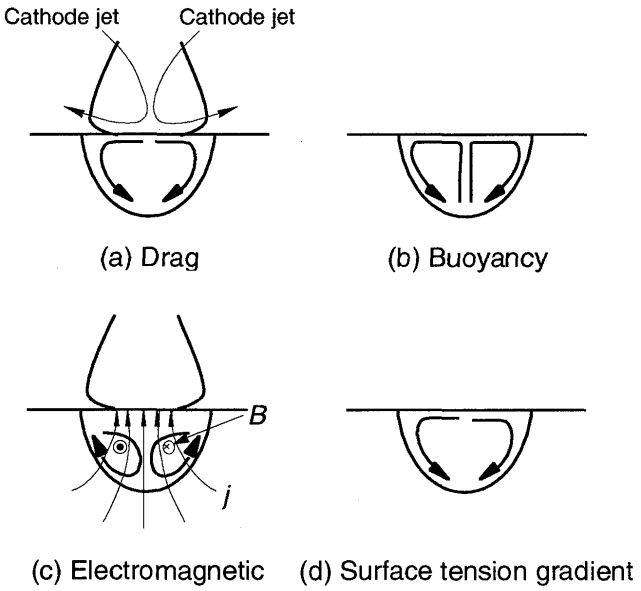

Fig. 1 Flow directions induced by four possible driving forces in the weld pool.

The governing equations, boundary conditions and numerical method are given in Sansonnens et al [16], therefore only the most pertinent details are outlined here. The mass continuity equation is

$$\frac{1}{r}\frac{\partial}{\partial r}(r\rho v_r)+\frac{\partial}{\partial z}(\rho v_z)=0 \qquad (1)$$

The radial momentum conservation equation is

$$\frac{1}{r}\frac{\partial}{\partial r}(r\rho v_r^2)+\frac{\partial}{\partial z}(\rho v_z v_r)=-\frac{\partial P}{\partial r}-j_z B_\theta +$$

$$\frac{1}{r}\frac{\partial}{\partial r}\left(2r\eta\frac{\partial v_r}{\partial r}\right)+\frac{\partial}{\partial z}\left(\eta\frac{\partial v_r}{\partial z}+\eta\frac{\partial v_z}{\partial r}\right)-2\eta\frac{v_r}{r^2} \qquad (2)$$

The axial momentum conservation equation is

$$\frac{1}{r}\frac{\partial}{\partial r}(r\rho v_r v_z)+\frac{\partial}{\partial z}(\rho v_z^2)=-\frac{\partial P}{\partial r}+j_r B_\theta +$$

$$\frac{\partial}{\partial z}\left(2\eta\frac{\partial v_z}{\partial z}\right)+\frac{1}{r}\frac{\partial}{\partial r}\left(r\eta\frac{\partial v_r}{\partial z}+r\eta\frac{\partial v_z}{\partial r}\right)+\rho g \qquad (3)$$

The energy conservation equation is

$$\frac{1}{r}\frac{\partial}{\partial r}(r\rho v_r h)+\frac{\partial}{\partial z}(\rho v_z h)=\frac{1}{r}\frac{\partial}{\partial r}\left(\frac{r\kappa}{c_p}\frac{\partial h}{\partial r}\right)+$$

$$\frac{\partial}{\partial z}\left(\frac{\kappa}{c_p}\frac{\partial h}{\partial z}\right)+j_r E_r+j_z E_z-U \qquad (4)$$

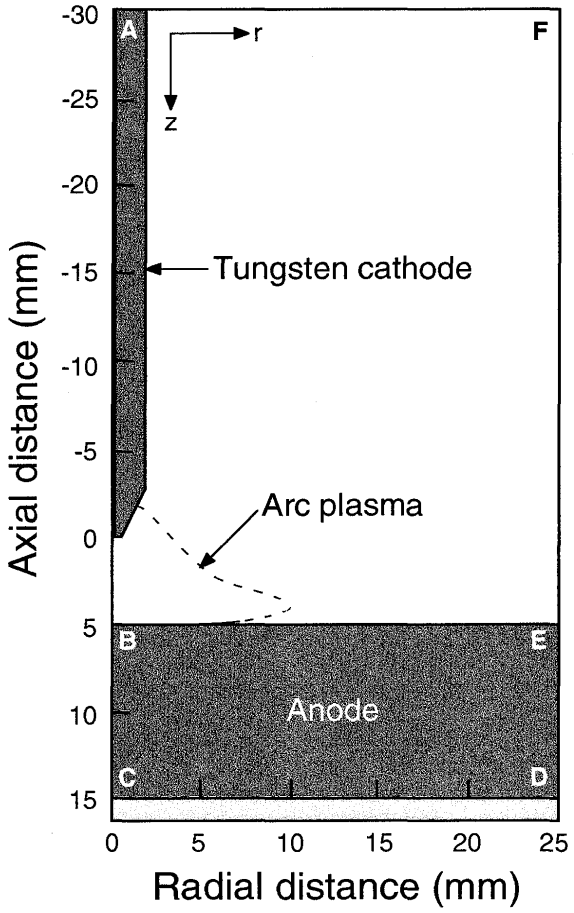

Fig. 2 Schematic illustration of calculated domain.

The current continuity equation is

$$\frac{1}{r}\frac{\partial}{\partial r}(rj_r)+\frac{\partial}{\partial z}(j_z)=0 \qquad (5)$$

where each physical symbol in the above equations indicates the same meaning as general use. Instead of the usual representation of the current density as dependent only on the electric field by Ohm's law ($j=\sigma E$), we also include a term to account for diffusion current from electrons. This term overcomes the problem that the equilibrium electrical conductivity is effectively zero in the plasma close to the electrodes owing to the low plasma temperature. This diffusion term is also consistent with our previous paper, which suggested that the diffusion current would dominate the arc current in the anode boundary layer [17]. Thus,

$$j_r=-\sigma\frac{\partial V}{\partial r}+eD_e\frac{\partial n_e}{\partial r} \qquad (6)$$

and

$$j_z=-\sigma\frac{\partial V}{\partial z}+eD_e\frac{\partial n_e}{\partial z} \qquad (7)$$

where D_e is the electron diffusion coefficient. The azi-

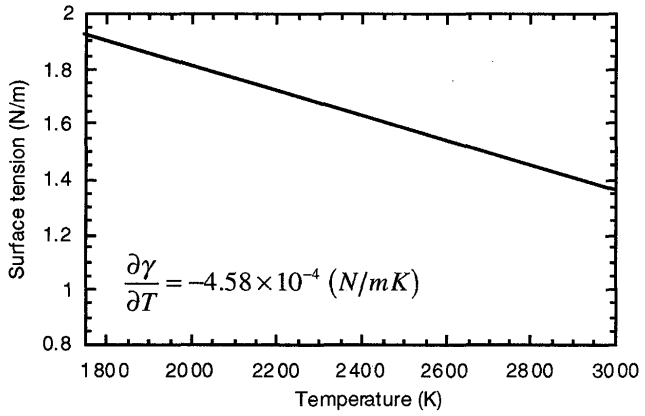

Fig. 3 Assumption of surface tension of molten SUS304.

muthal magnetic field B_θ induced by the arc current is evaluated by Maxwell's equation,

$$\frac{1}{r}\frac{\partial}{\partial r}(rB_\theta) = \mu_0 j_z \tag{8}$$

The electron continuity equation in terms of ambipolar diffusion is

$$\frac{1}{r}\frac{\partial}{\partial r}\left(rD_{amb}\frac{\partial n_e}{\partial r}\right)+\frac{\partial}{\partial z}\left(D_{amb}\frac{\partial n_e}{\partial z}\right)$$

$$+\psi\left[K_{eq}(T)n_e n_a - {n_e}^3\right]=0 \tag{9}$$

where D_{amb} is the ambipolar coefficient evaluated using the data of Devoto [18,19], $K_{eq}(T)$ is the Saha function, ψ is the three-body recombination coefficient [20,21].

Calculations at points on both electrode surfaces would need to include the special process occurring at the surfaces. Thus, additional energy flux terms need to be included in equation (4) at each electrode surface for thermionic heating and cooling from the electrons, ion heating, and radiation cooling. The additional energy flux for the cathode H_K and for the anode H_A are

$$H_K = -\varepsilon\alpha T^4 - |j_e|\phi_K + |j_i|V_i \tag{10}$$

and

$$H_A = -\varepsilon\alpha T^4 + |j|\phi_A \tag{11}$$

respectively. Here ε is the surface emission, α is the Stefan-Boltzmann constant, ϕ_K is the work function of the tungsten cathode, ϕ_A is the work function of the anode, and V_i is the ionization potential of argon.

At the anode surface, BE in Fig. 2, there are two sources of radial momentum as shown in Fig. 1. The first is the drag force, namely, the shear stress which is applied by the cathode jet on the surface of the weld pool, and the second is the surface tension gradient force, namely, the Marangoni force. The drag force is already reflected in equation (2) for the radial momentum conservation. The viscosity η makes the drag force at the anode surface. Therefore, the Marangoni force would need to be included in the radial momentum conservation at points on the anode surface, BE. In most cases, the difference in surface tension arises from the temperature variation at the weld pool surfaces [10], and then the Marangoni force ξ can be expressed by

$$\xi = -\eta\frac{\partial v_r}{\partial z} = \frac{\partial\gamma}{\partial T}\frac{\partial T}{\partial r} \tag{12}$$

where γ is the surface tension of the weld pool. Therefore, the additional term for equation (2) at the anode surface is

$$\text{Anode } F_A = \frac{\partial}{\partial z}\left(\frac{\partial\gamma}{\partial T}\frac{\partial T}{\partial r}\right) \quad . \tag{13}$$

In the present paper, we assumed that the anode was a stainless steel SUS304 and the surface tension of molten SUS 304 linearly decreased with temperature increase as shown in **Fig. 3** [9]. However, we were able to change the anode materials easily, and then we also used a copper as the anode for some comparisons with experiments, for example, comparison of the plasma temperatures with those values of experiment

The differential equations (1) to (9) are solved iteratively by the SIMPLEC numerical procedure [22].

3. Results and Discussion

In our model, we assumed that the melting point of the stainless steel was 1750 K. **Figure 4** represents a two-dimensional distribution of temperature in the whole region of the stationary GTA welding for a 150 A welding current. The maximum temperatures of the tungsten cathode, arc plasma and weld pool are ~3500 K at the tip of the cathode, 17000 K on the arc axis close to the cathode tip, and 2000 K at the center of the anode surface, respectively. **Figure 5** represents a two-dimensional distribution of fluid flow velocity. The interaction of the arc current with its own magnetic field leads to the phenomena of induced mass flow from the cathode to the anode. This induced mass flow is generally called the cathode jet [23]. The maximum calculated velocity of the cathode jet reaches 203 m s^{-1}. This cathode jet changes its direction in front of the anode surface, and then its radial component of the fluid flow drags the surface of the weld pool. This drag force is one of the driving forces of outward fluid flow in the weld pool. The outward fluid flow is also caused by a negative temperature coefficient of surface tension assumed in Fig. 3. The fluid flow caused by the surface tension gradient force is called the Marangoni convection. Figure 5 represents a numerical

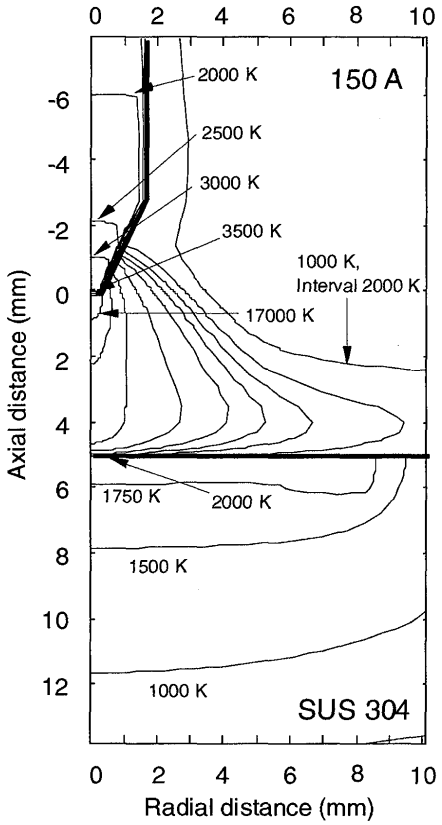

Fig. 4 Calculated temperature contours for a 150 A, stationary GTA welding of SUS304.

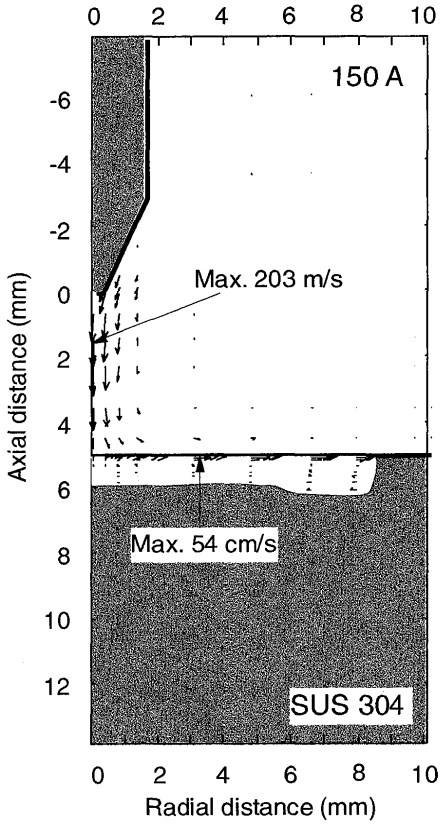

Fig. 5 Calculated fluid flow velocity for a 150 A , stationary GTA welding of SUS304.

result corresponding to outward fluid flow with a wide and shallow weld penetration which is a typical geometry in GTA welding process. The maximum calculated velocity in the weld pool for all considered cases in Fig. 1 reaches 54 cm s^{-1}, while the calculated convective flow in the weld pool was mainly dominated by the drag force of the cathode jet and the Marangoni force as compared with other two driving forces, namely, the buoyancy force and the electromagnetic force.

A comparison of the calculated temperature contours with experimental values of our previous paper [24] is made in **Fig. 6**. The experiment for a 150 A arc with the water cooled copper anode was carried out by the laser scattering measurement. It is seen that the predicted maximum temperature, as well as the other temperature, is in good agreement with the experiment. **Figure 7** shows the surface temperature of the cathode compared with experimental values of Zhou and Heberlein [25]. It is also seen that the predicted temperature is in good agreement with the experiment.

Stationary GTA welding was performed for comparison of the weld penetration with a calculated result. The experimental setup is shown in **Fig. 8**. The experiment was made for 20 seconds of arcing in the same conditions as the calculation. The anode was a disk (50 mm in diameter and 10 mm in thickness) of SUS 304 that was mounted into the

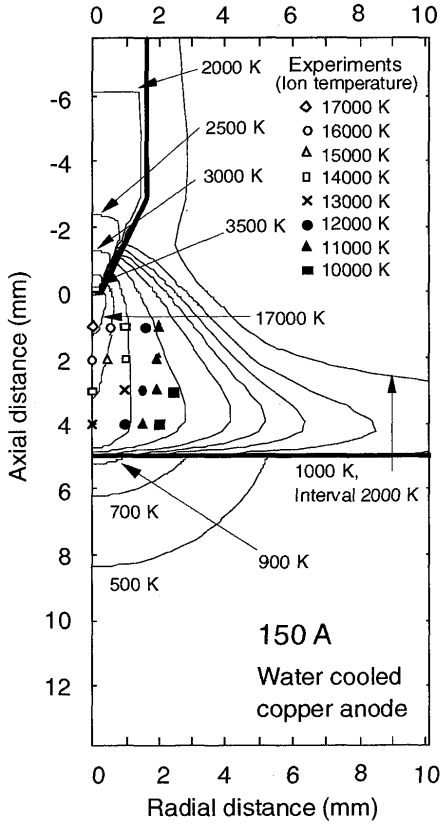

Fig. 6 Comparison of theoretical results in plasma temperature with experimental results of Tanaka (1999).

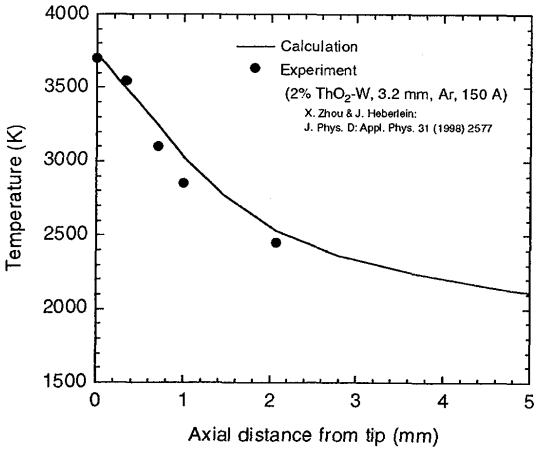

Fig. 7 Comparison of theoretical result of cathode temperature with experimental results of Zhou (1998).

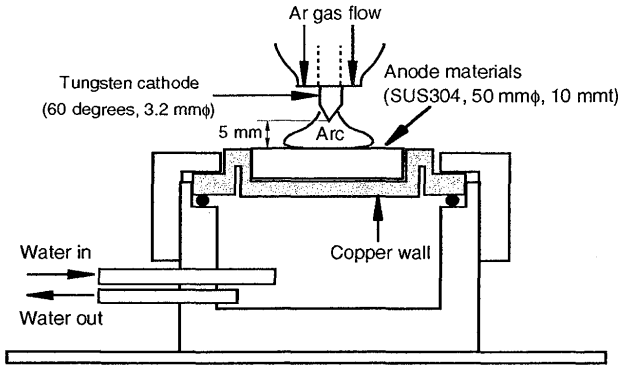

Fig. 8 Schematic illustration of the apparatus for stationary GTA welding of SUS304.

water cooled copper wall. The W-2% La_2O_3 electrode (diameter 3.2 mm with conical tip angle 60°) was used with a 5 mm arc length. The argon was employed as shielding gas at flow rate of 15 L/min. **Figure 9** shows the calculated weld penetration compared with the experimental result. There is approximate agreement between the calculated and experimental geometric shapes of weld penetration, although there is a difference between the calculated and experimental volumes of the weld. It is possible that the differences of physical properties taken from the literature [26-28] of thermal conductivity, specific heat, and viscosity as a function of temperature, particularly for the liquid metal, and those of the SUS 304 used in our experiment, would account for the differences in penetration volume. Furthermore, the theoretical predictions do not account for the depression of the weld pool surface by the arc pressure. The depression effect should change the drag force of the cathode jet at the weld pool surface. More discussion about the interaction between the arc plasma and the weld pool is necessary for solving this problem.

4. Conclusions

The conclusions in this paper are summarized as follows.

1) The whole region of GTA welding, namely, tungsten cathode, arc plasma, work-piece and weld pool has been treated in a unified numerical model.
2) The predicted two-dimensional distributions of temperature and velocity were shown, together with the predicted shape of the weld for a 150 A arc in argon. There was approximate agreement of weld shape with experiment.

References

1) M. Tanaka, T. Shimizu, H. Terasaki, M. Ushio, F. Koshi-ishi and C. L. Yang: Science and Technology of Welding and Joining, 5 (2000), 397.
2) A. Matsunawa: Proceedings of the 3rd International Conference on Trends in Welding Research, Gatlinburg, Tennessee, USA, June 1-5, 1992.
3) K. C. Hsu, and E. Pfender: J. Appl. Phys., 54 (1983) 4359.
4) P. Kovitya and J. J. Lowke: J. Phys. D: Appl. Phys. 18 (1985), 53-70.

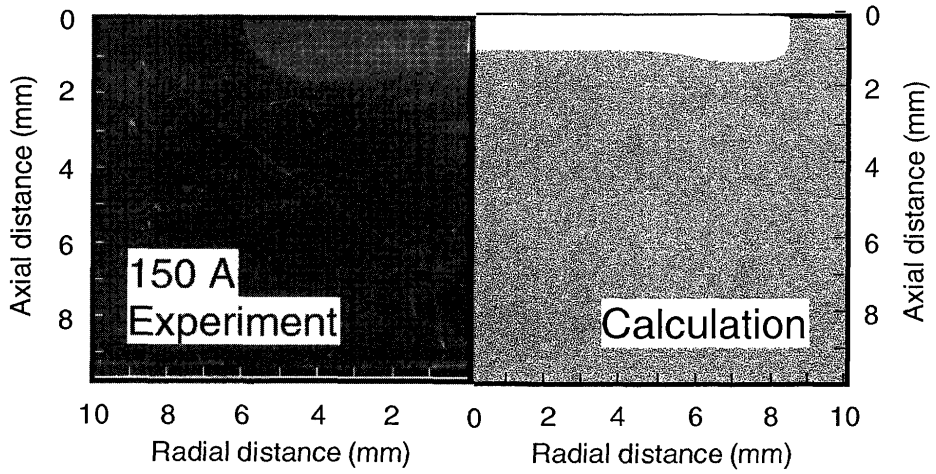

Fig. 9 Comparison of calculated result of weld penetration geometry with experimental result for a 150 A, stationary GTA welding of SUS304.

5) M. Ushio, J. Szekely, and C. W. Chang: Ironmaking and Steelmakimg, No.6 (1981) 279.
6) J. J. Lowke, P. Kovitya and H. P. Schmidt: J. Phys. D: Appl. Phys. 25 (1992), 1600.
7) C. S. Wu, M. Ushio and M. Tanaka: Computational Materials Science, 7 (1997), 308-314.
8) M. Goodarzi, R. Choo and J. M. Toguri: J. Phys. D: Appl. Phys. 30 (1997), 2744.
9) T. Zacharia, S. A. David, J. M. Vitek and T. Debroy: Metal. Trans. B, 21B (1990), 600.
10) S. A. David, T. DebRoy and J. M. Vitek: MRS Bulletin, 19 (1994), 29.
11) T. Zacharia, S. A. David, J. M. Vitekand H. G. Kraus: Welding Research Supplement, November 1995, 353.
12) Y. Lei, Y. Shi, H. Murakawa and Y. Ueda: Trans. JWRI, Joining and Welding Research Institute of Osaka University, 26 (1997), 1-8.
13) C. Winkler, G. Amberg, H. Inoue, T. Koseki and M. Fuji: Sci. and Tech. Welding and Joining, 5 (2000), 8-20.
14) R. T. C. Choo and J. Szekely: Welding Research Supplement, March 1992, 77.
15) M. Goodarzi, R. Choo, T. Takasu and J. M. Toguri: J. Phys. D: Appl. Phys. 31 (1998), 569.
16) L. Sansonnens, J. Haidar and J. J. Lowke: J. Phys. D: Appl. Phys. 33 (2000), 148.
17) M. Tanaka, M. Ushio and C. S. Wu: J. Phys. D: Appl. Phys. 32 (1999), 605.
18) R. S. Devoto: Phys. Fluids, 10 (1967), 354.
19) R. S. Devoto: Phys. Fluids, 10 (1967), 2105.
20) M. I. Hoffert and H. Lien: Phys. Fluids, 10 (1967) 1769-77.
21) E. Hinnov and J. G. Hirschberg: Phys. Rev. 125 (1962), 795-801
22) S. V. Patanker: Numerical Heat Transfer and Fluid Flow, Hemisphere Publishing Corporation.
23) M.H. Hirsh and H.J. Oskam: Gaseous Electronics, Academic Press, New York (1978).
24) M. Tanaka and M. Ushio: J. Phys. D: Appl. Phys. 32 (1999), 1153.
25) X. Zhou and J. Heberlein: J. Phys. D: Appl. Phys. 31 (1998), 2577.
26) J. F. Elliott and M. Gleiser: Thermochemistry for Steelmaking, Vol. 1, Addison-Wesley (1960).
27) The Japan Inst. Metals: Data-book for Metals, Maruzen, Tokyo (1984) (in Japanese).
28) Japan Stainless Steel Association: Handbook of stainless steel, The Nikkan Kogyo Shimbun, Tokyo (1995) (in Japanese).